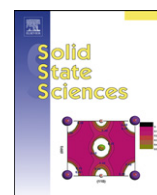


This article appeared in a journal published by Elsevier. The attached copy is furnished to the author for internal non-commercial research and education use, including for instruction at the authors institution and sharing with colleagues.

Other uses, including reproduction and distribution, or selling or licensing copies, or posting to personal, institutional or third party websites are prohibited.

In most cases authors are permitted to post their version of the article (e.g. in Word or Tex form) to their personal website or institutional repository. Authors requiring further information regarding Elsevier's archiving and manuscript policies are encouraged to visit:

<http://www.elsevier.com/copyright>



Ab initio investigations of the perovskite and K_2NiF_4 phases in the Cs–Ca–H system

S.F. Matar^{a,*}, M. Nakhl^b, A.F. Al Alam^c, M. Zakhour^b, N. Ouaini^c

^a CNRS, University of Bordeaux, ICMCB, 87 avenue du Docteur Albert Schweitzer, 33600 Pessac, France

^b Université Libanaise, Faculté des Sciences, Laboratoire de Chimie-Physique des matériaux (LCPM), Fanar, Lebanon

^c Université Saint Esprit de Kaslik, Faculté des Sciences, URA GREVE, Jounieh, Lebanon

ARTICLE INFO

Article history:

Received 24 November 2010

Accepted 8 December 2010

Available online 16 December 2010

This paper is dedicated to Bernard Darriet and to the memory of Michel Pezat.

Keywords:

Ionic hydrides

Cs–Ca–H system

DFT

VASP

ASW

PAW-GGA

ABSTRACT

Deriving the energy–volume equation of state within DFT for $CsCaH_3$ and Cs_2CaH_4 has allowed predicting significant changes within the ionic behavior of hydrogen. In Cs_2CaH_4 , apical H1 and equatorial H2 are found as less and more ionic respectively as compared to the perovskite hydride. This leads to a larger overall binding both from energy differences and chemical bonding analysis.

© 2010 Elsevier Masson SAS. All rights reserved.

1. Introduction

Several binary and ternary ionic hydrides exist; many of them based on alkali- and alkaline-earth metals. They are characterized by nearly fully anionic hydrogen and large band gaps. The strong bonding of hydrogen with the metal matrix such as in MgH_2 hinders their use as hydrogen storage for energy sources under normal conditions. However they are envisaged for such applications at elevated temperatures [1].

The original investigations within the Cs–Ca–H system by Park, Pezat and Darriet [2] suggested the existence of $CsCaH_3$ with orthorhombic $GdFeO_3$ -type perovskite structure. However Bronger and Breil [3] proposed that the synthesized phase was actually Cs_2CaH_4 with a K_2NiF_4 -type structure, and provided X-ray diffraction analysis with atomic positions. The structure is shown in Fig. 1 with corner sharing CaH_6 octahedra interlayered with CsH rocksalt like entities. Hereafter, the apical hydrogen is called H1 and the equatorial one, H2. Nevertheless a cubic perovskite was identified later on by Gingl et al. [4]. On the electronic structure side, a number of ternary hydrides with perovskite structure were investigated by

Sato et al. [5]. In view of the presence of two ternary hydrides within the Cs–Ca–H ternary, $CsCaH_3$ and Cs_2CaH_4 , we engaged a comparative study of their electronic structure for establishing trends of stability and change of ionic behavior of hydrogen, using complementary computational methods within the well established quantum theoretical density functional DFT [6].

2. Computational methodology

Within DFT, a pseudo-potential approach within the VASP code [7,8] is used firstly to geometry optimize atomic positions and lattice parameters. Then the respective equations of states (EOS) are obtained through energy–volume curves fitted with Birch EOS [9]. For these purposes, we use the accurate projector augmented wave (PAW) method [8,10] with potentials built within the generalized gradient approximation (GGA) for an account of the effects of exchange and correlation [11]. The calculations are converged at an energy cut-off of 95.45 eV for cubic perovskite $CsCaH_3$ and 159 eV for Cs_2CaH_4 . The k -point integration is carried out with a starting mesh of $4 \times 4 \times 4$ up to $8 \times 8 \times 8$ for best convergence and relaxation to zero strains. The Brillouin zone integrals are approximated using a special k -point sampling following Blöchl [10].

For a full description of the electronic band structures and of chemical bonding, the scalar relativistic all-electrons augmented

* Corresponding author.

E-mail addresses: matar@icmcb-bordeaux.cnrs.fr, s.matar@u-bordeaux1.fr (S.F. Matar).

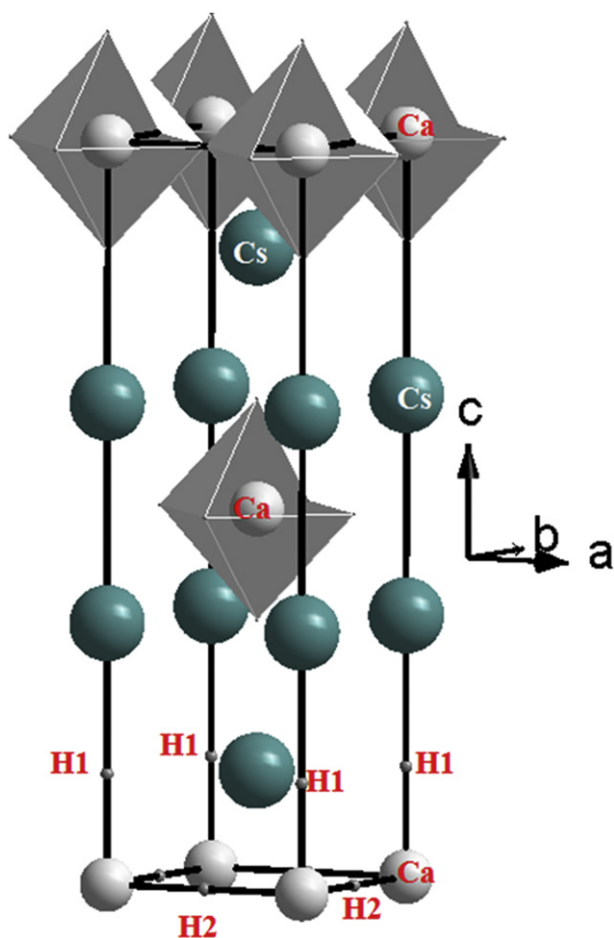


Fig. 1. The body centered tetragonal structure of Cs_2CaH_4 .

spherical wave (ASW) [12,13] method is used. Like in the calculations with pseudo-potentials, the exchange and correlation effects are accounted for within GGA functional [11]. In the ASW method, the wave function is expanded in atom-centered augmented spherical waves, which are Hankel functions and numerical solutions of Schrödinger's equation, respectively, outside and inside the so-called augmentation spheres. In order to optimize the basis set, additional augmented spherical waves are placed at carefully selected interstitial sites (IS). The choice of these sites as well as the augmentation radii are automatically determined using the sphere-geometry optimization algorithm [14]. Self-consistency is achieved by a highly efficient algorithm for convergence acceleration [15]. The Brillouin zone integrations are performed using the linear tetrahedron method [10]. In the minimal ASW basis set, we have chosen the outermost shells to represent the valence states using partial waves up to $l_{\text{max}} + 1 = 2$ for Ca, Cs, H and IS. The completeness of the valence basis set is checked for charge convergence. The self-consistent field calculations are run to a convergence of $\Delta Q = 10^{-8}$ for the charge density and the accuracy of the method is in the range of about 10^{-7} eV regarding energy differences. The relative magnitude of the chemical bonding is obtained based on the covalent bond energy ECOV approach which merges both overlap and Hamiltonian population analysis (resp. S_{ij} , and H_{ij} , i, j being two chemical species) [16]. The ECOV are constructed by considering s and p-like valence states of Cs, Ca and H. In the plots negative, positive and zero ECOV magnitudes indicate bonding, anti-bonding and non-bonding interactions respectively.

3. Geometry optimization and equations of state

Starting from the internal lattice coordinates of literature for the ternary hydrides [3,4], we carried out a full geometry optimization. The optimized lattice parameters, shown in Tables 1 and 2, are in good agreement with experimental data. Also the Ca–H distances are smaller than Cs–H ones in both varieties. It will be shown hereafter that they indicate prevailing Ca–H bonding which is differentiated between the two H sites in the K_2NiF_4 -type structure of Cs_2CaH_4 .

3.1. Equations of state

In order to extract energies to compare the binding within the two ternary hydrides, one needs establishing the energy–volume equation of state (EOS). In fact the calculated total energy pertains to the cohesive energy within the crystal because the solution of the Kohn–Sham DFT equations yield the energy with respect to infinitely separated electrons and nuclei. In as far as the zero of energy depends on the choice of the pseudo-potentials, somehow it becomes arbitrary; i.e. it is shifted but not scaled. However the energy derivatives as well as the EOS remain unaltered. For this reason one needs to establish the EOS and extract the fit parameters for an assessment of the equilibrium values. This is done from (E,V) set of calculations around minima found from geometry optimization. The resulting $E = f(V)$ curves have a quadratic variation which can be fitted with energy–volume Birch EOS to the 3rd order [12]:

$$E(V) = E_0(V_0) + [9/8]V_0B_0 \left[\left(\frac{V_0}{V} \right)^{2/3} - 1 \right]^2 + [9/16]B_0(B' - 4)V_0 \left[\left(\frac{V_0}{V} \right)^{2/3} - 1 \right]^3,$$

where E_0 , V_0 , B_0 and B' are the equilibrium energy, the volume, the bulk modulus and its pressure derivative, respectively.

Also for a test of Park et al. hypothesis of a GdFeO_3 -type CsCaH_3 [2] its EOS was calculated beside the cubic one. The two curves together with the fit results in the inserts are shown in Fig. 2a. In this panel and in following ones relevant to the EOS, low residue χ^2 values ($\sim 10^{-6}$) are indicative of good fits. It can be seen that the system is slightly more stable in the cubic structure with a volume per formula unit (fu) in closer agreement with experiment than from geometry optimized value in Table 1. In as far as the main difference between cubic perovskite and orthorhombic one is in the tilting of the CaH_6 octahedra in the latter which is a stabilizing factor leading eventually to a transformation to post-perovskite in oxides (covalent) under pressure [17], then (ionic) hydride systems behave oppositely; i.e. a non tilted sequence of octahedra is preferred. The zero pressure bulk modulus of $B_0 = 23$ GPa (in both varieties), is in agreement with literature [5]. It indicates a soft, highly compressible material in comparison with oxides based on transition metals [17], despite the three dimensional structure. Note that all chemical elements in presence are s-like, i.e. with non directional (p or d) orbitals.

Table 1

Crystal characteristics of cubic perovskite CsCaH_3 from geometry and comparison with literature data.

CsCaH_3 $Pm-3m$ #221 $Z = 1$	This work	Ref. [4]
Cs	0, 0, 0	0, 0, 0
Ca	$\frac{1}{2}, \frac{1}{2}, \frac{1}{2}$	$\frac{1}{2}, \frac{1}{2}, \frac{1}{2}$
H	$\frac{1}{2}, \frac{1}{2}, 0; 0, \frac{1}{2}, \frac{1}{2}; \frac{1}{2}, 0, \frac{1}{2}$	$\frac{1}{2}, \frac{1}{2}, 0; 0, \frac{1}{2}, \frac{1}{2}; \frac{1}{2}, 0, \frac{1}{2}$
a (Å)	4.54	4.61
Volume (Å ³)	80.0	97.9
d (Ca–H) (Å)	2.29	2.30
d (Cs–H) (Å)	3.12	3.15

Table 2
Crystal characteristics of K_2NiF_4 -type Cs_2CaH_4 from geometry and comparison with literature data.

Cs_2CaH_4 $I4/mmm$ #139 $Z = 2$	This work	Ref. [3]
Cs	0, 0, 0.351	0, 0, 0.352
Ca	0, 0, 0	0, 0, 0
H1	0, 0, 0.151	0, 0, 0.149
H2	0, ½, 0	0, ½, 0
a (Å)	4.58	4.597
c (Å)	15.271	15.528
Volume (Å ³)	320.33	328.14
d(CaH1) (Å)	2.30	2.31
d(Ca–H2) (Å)	2.27	2.29
d(Cs–H1) (Å)	3.12	3.15
d(Cs–H2) (Å)	3.23	3.25

In Fig. 2b relevant to the $E(V)$ curves and fit values for Cs_2CaH_4 hydride, the system is found softer with a very small value of bulk modulus of 16 GPa. One may attribute the results to the known difference of dimensionality (D) between the perovskite and K_2NiF_4 -type structures which are respectively 3D and 2D-like. The equilibrium volume shows a fairly good agreement with experiment.

3.2. Binding energies

From the equilibrium values one may estimate the relative cohesive energies for the two ternary hydride systems starting from those of CsH and CaH_2 . As a matter of fact the ternary hydrides are

experimentally prepared by reacting these binaries [2]. The former crystallizes in rocksalt structure while for the latter different reports exist on its structure: fluorite CaF_2 -like [18] and orthorhombic [19]. In this context we calculated the EOS in the three structural types to obtain the ground state structure. For the sake of completeness, a rutile MgH_2 -like structure was also considered. Fig. 3a shows the three $E(V)$ curves and the fit values in the inserts; the goodness of fit is indicated by a low χ^2 value. The most stable structural type is CaF_2 , followed by the orthorhombic then rutile types. This is supported by Weaver et al. work on experimental and theoretical investigations of CaH_2 [18]. The EOS of CsH in the ground state rocksalt NaCl structure is given in Fig. 3b. The bulk modulus value of CsH and CaH_2 are respectively smaller and larger than the magnitudes of the ternary systems. Interestingly, “adding” CsH to $CsCaH_3$ ($B_0 = 23$ GPa) yields a much softer Cs_2CaH_4 ($B_0 = 16$ GPa) material.

The binding within each system can be obtained from the equation:

$$E_{\text{bind.}}(CsCaH_3) = E_{\text{tot.}}(CsCaH_3) - E_{\text{tot.}}(CsH) - E_{\text{tot.}}(CaH_2);$$

and

$$E_{\text{bind.}}(Cs_2CaH_4) = E_{\text{tot.}}(Cs_2CaH_4) - 2 E_{\text{tot.}}(CsH) - E_{\text{tot.}}(CaH_2).$$

With the equilibrium zero pressure values in the inserts one gets $E_{\text{bind.}}(CsCaH_3) = -0.03$ eV and $E_{\text{bind.}}(Cs_2CaH_4) = -0.1$ eV, i.e. a three times larger magnitude. The larger binding within the K_2NiF_4 -type

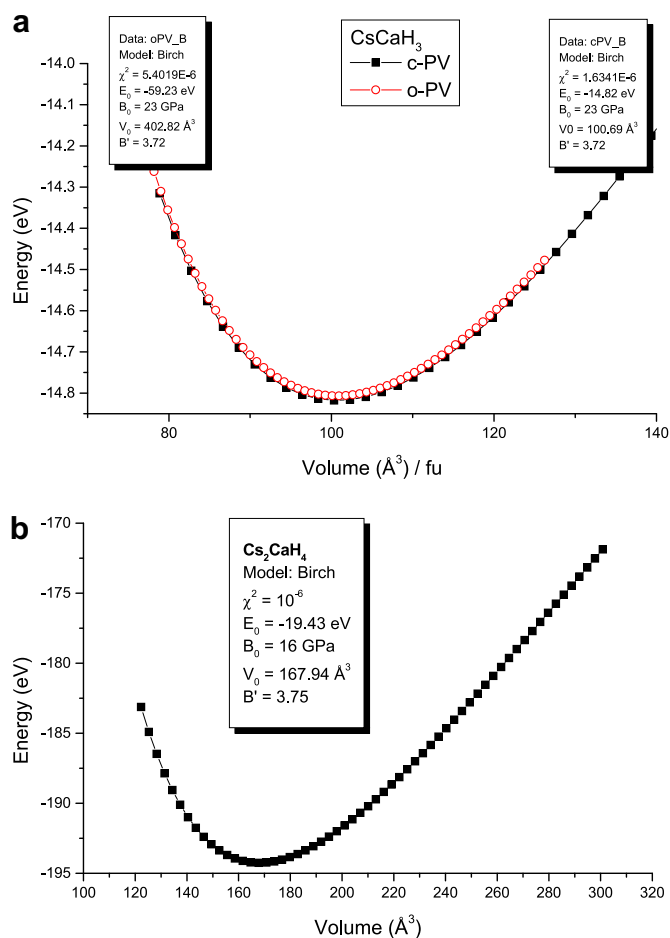


Fig. 2. Energy versus volume curves and fit values from Birch 3rd order equation state. a) $CsCaH_3$ and b) Cs_2CaH_4 . χ^2 indicates the goodness of fit.

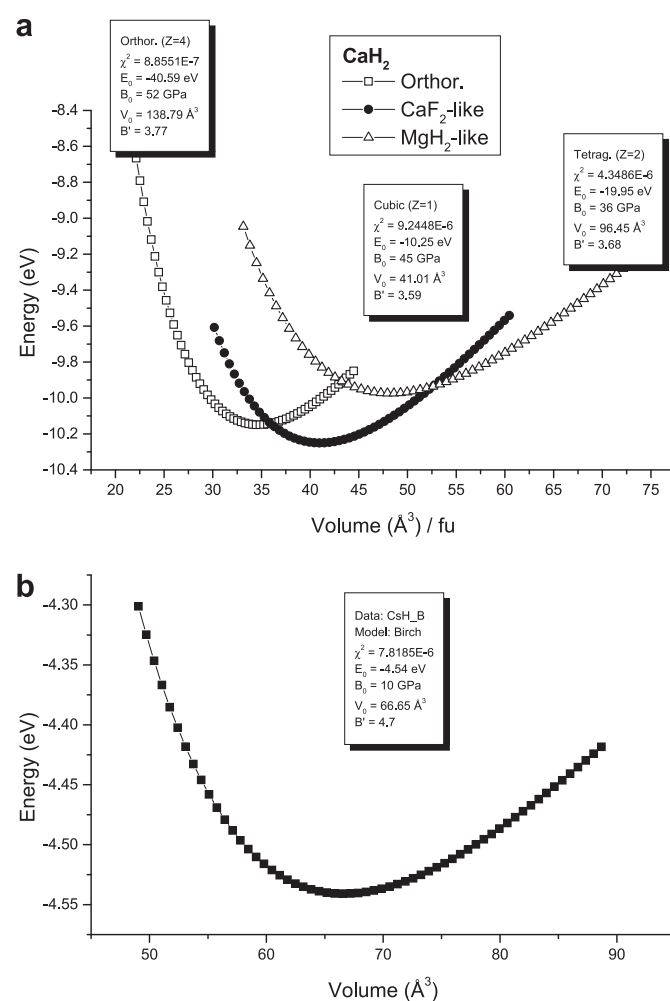


Fig. 3. Energy versus volume curves and fit values from Birch 3rd order equation state. a) CaH_2 and b) CsH. χ^2 indicates the goodness of fit.

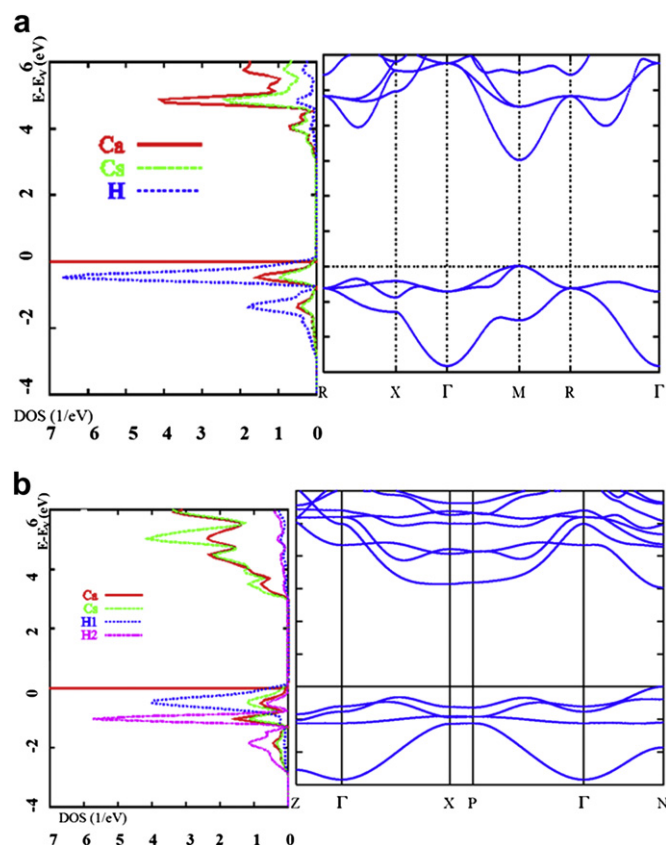


Fig. 4. Site projected density of states and electronic band structure along major Brillouin zone lines of CsCaH₃ (a) and Cs₂CaH₄ (b).

hydride should find its interpretation from the chemical binding changes which are addressed here below.

4. Electronic structure and chemical bonding

Using the optimized lattice positions for the two ternary hydrides (Tables 1 and 2), we calculate the electronic structures and the properties of chemical bonding for both varieties with all-electrons ASW method [12,13]. At self-consistent convergence, charge transfer is observed from Ca and Cs towards H and IS with amounts of ~ 0.5 electron. These transfers are not meaningful of fully ionized elements; such features will be indirectly shown through the electronic band structure and density of states as well as the chemical bonding properties.

4.1. Electronic band structure and density of states

The site projected density of states (PDOS) and the corresponding bands on the right hand side (RHS) are shown in Fig. 4 for both ternary hydrides. They are both insulating with a large band gap of ~ 3 eV. This is close to the gap magnitude in the literature for the perovskite hydride [5]. Then the energy values along the y-axis are with respect to the top of the valence band (VB), E_V . This is also done in following plots. Within the VB, one finds bands arising from hydrogen 1s with three bands in CsCaH₃ (Fig. 4a) and four bands in Cs₂CaH₄ (Fig. 4b). In O_h point group they correspond to the following symmetric irreducible representations: a_{1g} (one-degenerate) and e_g (two-degenerate) with respectively large and little dispersion of the bands. In Cs₂CaH₄, the point group at Ca is D_{4h} and the following symmetric irreducible representations apply to assign the four bands: a_{1g} and a_{2g} and e_g . It is interesting to notice the small dispersive a_{2g} band giving the high intensity DOS peak at ~ -1 eV, mainly assigned to H2. In both panels the large band dispersion is at the center of the Brillouin zone (Γ). The bands give the PDOS their shape. And the similar PDOS shapes for Cs, Ca on

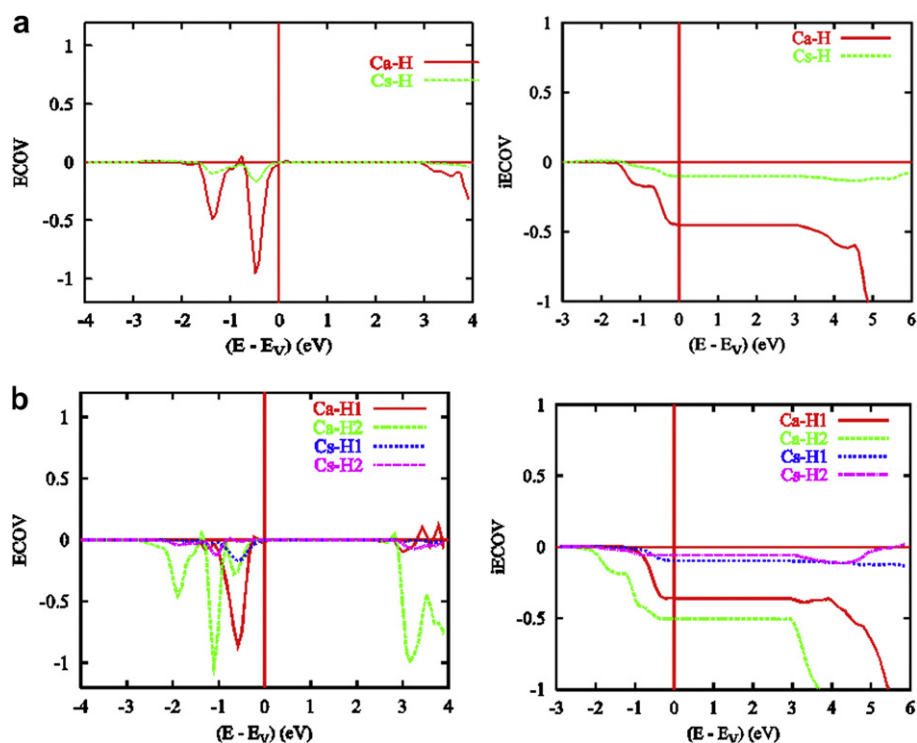


Fig. 5. Chemical bonding from ECOV and integrated iECOV; a) CsCaH₃; b) Cs₂CaH₄.

one hand and H on the other hand, signal a chemical bonding between them, detailed below. Despite similar magnitude of VB widths, i.e. ~ 3 eV, the hydrogen PDOS show differences between the two panels, with an overall energy downshift of H2 versus H1 PDOS in Cs₂CaH₄. This may be connected with the distances which are shortest for Ca–H2 (Table 2). The conduction band (CB) comprising mainly Cs and Ca empty states shows larger dispersion in Cs₂CaH₄ with respect to CsCaH₃. These observations indicate similar overall ionic character for both hydrides with a “redistribution” of hydrogen chemical roles in Cs₂CaH₄.

4.2. Chemical bonding

The discussion of the electronic band structure and PDOS can be developed from the description of the chemical bonding in the two ternary hydrides. This is based on the ECOV criterion. For sake of establishing trends of bonding strengths we also show the integrated ECOV function (*i*ECOV): the larger the area below the curves, the larger the bonding is. Further we consider the same number of atoms. The relevant plots are shown in Fig. 5a,b.

In both hydrides, the Ca–H bonding is stronger than the Cs–H one as one may expect from distance magnitudes (Tables 1 and 2). All interactions are of bonding character whence the negative ECOV all over and the ECOV follow closely the PDOS (and the bands). Differences appear between the two hydrides for the intensity of ECOV peaks at -0.5 eV (5a) and the onset of a peak at -2 eV in Fig. 5b. Further the bonding is of very low magnitude below ~ -1.8 eV in the perovskite hydride, while it is significant below this energy over a 1 eV range due to Ca–H2 bonding. Although the Ca–H2 ECOV peak intensity appears larger than Ca–H1 one, a comparison of the interactions is better illustrated from the integrated ECOV (*i*ECOV). The right hand side (RHS) panels show the relevant curves which exhibit again the low intensity Cs–H areas versus Ca–H. Comparing the relative intensities of the latter, one can see that the Ca–H bonding in the perovskite hydride (Fig. 5a, RHS) is found intermediate between Ca–H1 and Ca–H2 (Fig. 5b, RHS), i.e. there is the following trend of bonding:

$$i\text{ECOV}(\text{Ca-H1}/\text{Cs}_2\text{CaH}_4) < i\text{ECOV}(\text{Ca-H}/\text{CsCaH}_3) < i\text{ECOV}(\text{Ca-H2}/\text{Cs}_2\text{CaH}_4)$$

This has important implications from the chemical structure stand point: upon going from the perovskite to the K₂NiF₄ hydride, there is a dispatching of hydrogen into a less anionic H1 and a more anionic H2. This may explain the larger binding and stabilization of the K₂NiF₄ hydride with respect to the perovskite as calculated above.

5. Conclusion

The electronic structures of two ternary hydrides within the Cs–Ca–H system, has allowed pointing to significant changes affecting the ionic behavior of hydrogen from CsCaH₃ to Cs₂CaH₄. From the equilibrium energy values obtained with help of respective EOS, including CsH and CaH₂, the bonding is computed larger in the latter. This has been assessed based on the electronic band structures and chemical bonding leading to dispatch hydrogen into less and more ionic in Cs₂CaH₄ as with respect to H in CsCaH₃.

References

- [1] G. Renaudin, B. Bertheville, K. Yvon, J. Alloys Compounds 353 (2003) 175.
- [2] H.H. Park, M. Pezat, B. Darriet, Rev. Chim. Miner. 23 (1986) 323.
- [3] W. Bronger, L. Breil, Z. Anorg. Allg. Chem. 623 (1997) 119.
- [4] F. Gingl, T. Vogte, E. Akiba, K. Yvon, J. Alloys Compounds 282 (1999) 125.
- [5] T. Sato, D. Noréus, H. Takeshita, U. Häussermann, J. Solid State Chem. 178 (2005) 3381.
- [6] P. Hohenberg, W. Kohn, Phys. Rev. B. 136 (1964) 864; W. Kohn, L.J. Sham, Phys. Rev. A 140 (1965) 1133.
- [7] G. Kresse, J. Furthmüller, Phys. Rev. B. 54 (1996) 11169.
- [8] G. Kresse, J. Joubert, Phys. Rev. B. 59 (1999) 1758.
- [9] F. Birch, J. Geophys. Res. 83 (1978) 1257.
- [10] P.E. Blöchl, Phys. Rev. B. 50 (1994) 17953.
- [11] J. Perdew, K. Burke, M. Ernzerhof, Phys. Rev. Lett. 77 (1996) 3865.
- [12] A.R. Williams, J. Kübler, C.D. Gelatt, Phys. Rev. B. 19 (1979) 6094.
- [13] V. Eyert, “The Augmented Spherical Wave Method – A Comprehensive Treatment” Lecture Notes in Physics. Springer, Heidelberg, 2007.
- [14] V. Eyert, K.H. Höck, Phys. Rev. B. 57 (1998) 12727.
- [15] V. Eyert, J. Comput. Phys. 124 (1996) 271.
- [16] G. Bester, M. Fähnle, J. Phys. Condens. Matter 13 (2001) 11541.
- [17] S.F. Matar, G. Demazeau, A. Largeteau, Solid State Sci. 12 (2010) 373.
- [18] J.H. Weaver, M. Gupta, D.T. Peterson, Solid State Comm. 51 (1984) 805.
- [19] Ralph W.G. Wyckoff, Crystal Structure, Vol. 1, Interscience Publishers, 1963, p. 303.